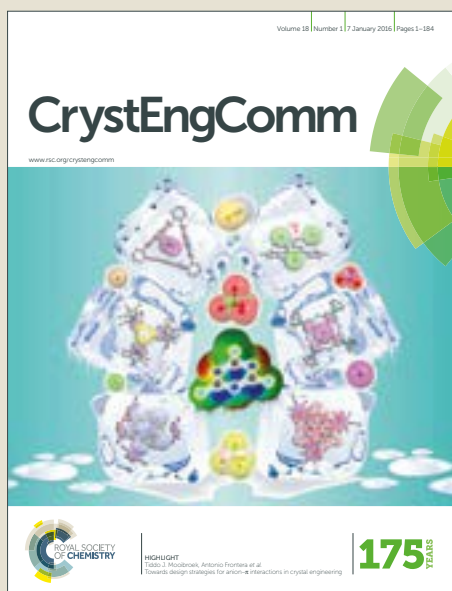


CrystEngComm

Accepted Manuscript



This article can be cited before page numbers have been issued, to do this please use: X. Kong, Y. Zhang, T. He, X. Wu, M. Xu, S. Wang, L. Xie and J. J. Li, *CrystEngComm*, 2018, DOI: 10.1039/C8CE00779A.



This is an Accepted Manuscript, which has been through the Royal Society of Chemistry peer review process and has been accepted for publication.

Accepted Manuscripts are published online shortly after acceptance, before technical editing, formatting and proof reading. Using this free service, authors can make their results available to the community, in citable form, before we publish the edited article. We will replace this Accepted Manuscript with the edited and formatted Advance Article as soon as it is available.

You can find more information about Accepted Manuscripts in the [author guidelines](#).

Please note that technical editing may introduce minor changes to the text and/or graphics, which may alter content. The journal's standard [Terms & Conditions](#) and the ethical guidelines, outlined in our [author and reviewer resource centre](#), still apply. In no event shall the Royal Society of Chemistry be held responsible for any errors or omissions in this Accepted Manuscript or any consequences arising from the use of any information it contains.



Journal Name

ARTICLE

Two interpenetrated metal-organic frameworks with a slim ethynyl-based ligand: designed for selective gas adsorption and structural tuning

Received 00th January 20xx,
Accepted 00th January 20xx

DOI: 10.1039/x0xx00000x

www.rsc.org/

Xiang-Jing Kong, Yong-Zheng Zhang, Tao He, Xue-Qian Wu, Ming-Ming Xu, Si-Nan Wang, Lin-Hua Xie, Jian-Rong Li*

In the design and construction of metal-organic frameworks (MOFs), the utilization of slim ligands is usually more inclined to form interpenetrated structures compared with bulky ones. The structural interpenetration can improve the framework stability, and in some cases enhance gas adsorption capacity and selectivity due to the confined pores. In order to explore the structural control of MOFs and construct new MOFs with good selective gas adsorption ability, herein a slim ethynyl-based 4-connected carboxylate acid ligand 4,4',4'',4'''-(benzene-1,2,4,5-tetrayltetrakis(ethyne-2,1-diyl))tetrabenzoic acid (H₄BTEB) was used to design and construct MOFs, hopefully having interpenetrated structures. Combining with 4-connected paddle-wheel Cu₂(COO)₄ and 8-connected Zr₆O₄(OH)₈(COO)₈ clusters, BTEB⁴⁻ ligand led to two new MOFs, [Cu₂(BTEB)(H₂O)₂] (BUT-43) and [Zr₆O₄(OH)₈(H₂O)₄(BTEB)₂] (BUT-44). As expected, the two MOFs have two-fold interpenetrated framework structures with partitioned channels. BUT-43 contains a rare three-dimensional (3D) 4-connected single network with a *1vt* topology, which then interpenetrates. While in BUT-44 each Zr₆-based cluster is coordinated with eight BTEB⁴⁻ ligands to give a single 3D 4,8-connected *scu* network, then it doubly interpenetrates to give the first example of interpenetrated 4,8-connected Zr(IV)-MOF. Studies on their stability and gas adsorption properties show that BUT-44 is highly stable to withstand pH = 10 NaOH and 1 M HCl aqueous solutions. And more interestingly, both MOFs represent good gas adsorption selectivities of C₂H₂ over CO₂ and CH₄, suggesting potential application in gas separation.

Introduction

Metal-organic frameworks (MOFs), emerging as a new class of versatile porous materials that are constructed from metal-based nodes connecting with organic linkers through coordination bonds, have received considerable attention in the past two decades due to their high crystallinity, extraordinary porosity, and diverse functionality.¹ The unique crystalline periodic networks of MOFs with tunable pore sizes and functionalities enable them to be promising materials with extensive applications such as in gas storage and/or separation, chemical sensing, drug delivery, and heterogeneous catalysis.²

The rational design of organic linkers and precise choice of metal-containing nodes are of great importance in order to obtain desired MOFs with specific structures and properties. From a

construction perspective, the ligand is a very significant building block because of the fact that its geometry and functionality will make a direct influence on the output of related MOFs, as well as generated metal clusters in some cases.³ In general, in the construction of MOFs, the utilization of slim (long and thin) ligands is more inclined to form interpenetrated structures with improved stability compared with bulky ones, and the non-interpenetrating frameworks based on big ligands are usually fragile and vulnerable to collapse.⁴ Simultaneously, interpenetrated frameworks also feature the additional advantage of enhanced size- and shape-selective effects toward guest molecules, and may thus enhance gas selective adsorption of resulting MOFs due to the confined pores.⁵ In addition, it has been demonstrated that the incorporation of functional groups, such as organic amine, hydroxyl, and C≡C triple bonds⁶ and inorganic SiF₆²⁻ and Cr₂O₇²⁻,⁷ into MOFs is able to increase the interactions between gas molecules and framework through van der Waals forces and/or π–π interactions as well as electrostatic interactions, thereby efficaciously tuning their gas adsorption property. As a special case, the introduction of ethynyl into the backbone of the polycarboxylate ligands could thus not only provide C≡C triple bonds as electron-donors but also enlarge

^a Beijing Key Laboratory for Green Catalysis and Separation and Department of Chemistry and Chemical Engineering, College of Environmental and Energy Engineering, Beijing University of Technology, Beijing 100124, P. R. China.
E-mail: jrli@bjut.edu.cn.

† Electronic Supplementary Information (ESI) available: ¹H NMR, FT-IR, TGA and crystal data (CCDC No.: 1842449 and 1842448). See DOI: 10.1039/x0xx00000x

the linkers in size, which is in favour of the formation of interpenetrated frameworks.

Beside of organic linkers, the structure and functionality of MOFs can also be largely affected by the compositions and structures of their metal-containing nodes with different elements, sizes, shapes, coordination numbers, and coordination modes.⁸ Square paddle-wheel $\text{Cu}_2(\text{COO})_4$ (as Cu_2 cluster) and dodecahedral $\text{Zr}_6\text{O}_8(\text{COO})_{12}$ clusters are among common secondary building units (SBUs) used in constructing a variety of MOFs, which sometimes exhibit intriguing structures and properties.⁹ Particularly, the unique geometry and high linkage number of the latter enable it to serve as various kinds of nodes in resultant networks by reducing the connectivity (as $\text{Zr}_6\text{O}_8(\text{COO})_n$, $n = 3, 6, 8, 9, 10, \text{ or } 12$, called Zr_6 cluster), which could be achieved through using different ligands and/or tuning synthetic conditions.¹⁰ $\text{Cu}(\text{II})$ paddle-wheel based MOFs have been widely investigated mainly for their mild synthetic conditions and accessible open metal sites on $\text{Cu}(\text{II})$ ions, which are favorable to gas storage, separation, and catalysis.¹¹ $\text{Zr}(\text{IV})$ -MOFs with unsaturated Zr_6 nodes have attracted enormous research interest, among of which the 8-connected Zr_6 cluster is most popular, due to their good stability and fascinating properties, thereby great application potential.¹² Thus, both Cu_2 and Zr_6 clusters are excellent SBU platforms for the rational design and structural tuning of MOFs in terms of given applications, such as for gas selective adsorption and separation. Nevertheless, it should be pointed out that the construction of desired MOFs with robust structures and suitable pores to discriminate different gases is somewhat a complicated process, for which both the smart strategy and abundant efforts are required for ever.

With above considerations, in this work, a slim and ethynyl-containing 4-connected ligand 4,4',4'',4'''-(benzene-1,2,4,5-tetrayltetraakis(ethyne-2,1-diyl))tetrabenzoic acid¹³ (H_4BTEB , Fig. 1a) has been used to assemble with Cu_2 and Zr_6 clusters, attempting to construct interpenetrated MOFs with enhanced stability and good gas selective adsorption property. As expected, two new MOFs, $[\text{Cu}_2(\text{BTEB})(\text{H}_2\text{O})_2]$ (BUT-43, BUT = Beijing University of Technology) and $[\text{Zr}_6\text{O}_4(\text{OH})_8(\text{H}_2\text{O})_4(\text{BTEB})_2]$ (BUT-44) were hydrothermally synthesized, whose 3D interpenetrated structures were revealed by single crystal X-ray diffractions (SXRD). To our knowledge, BUT-44 represents the first example of a 4,8-connected $\text{Zr}(\text{IV})$ -MOF with an interpenetrated structure. Furthermore, the stability and adsorption properties of them have been examined. The results show that BUT-44 has outstanding chemical stability, and both MOFs exhibit good gas adsorption selectivities of C_2H_2 over CO_2 and CH_4 , suggesting their potential application in gas separation.

Experimental

Materials and methods

All reagents (AR grade) were commercially purchased and used as received. ^1H NMR data were collected on a Bruker Avance III HD 400 MHz NMR spectrometer. Fourier-transform infrared (FT-IR) spectra were recorded on an IR Affinity-1 instrument. Thermogravimetric analyse (TGA) data were obtained on a TGA-50

thermogravimetric analyzer at a heating rate of $10\text{ }^\circ\text{C min}^{-1}$ under air atmosphere. The powder X-ray diffraction (PXRD) patterns were recorded on a Bruker D8-Focus Bragg-Brentano X-ray powder diffractometer equipped with a Cu sealed tube ($\lambda = 1.54178\text{ \AA}$) at room temperature (RT). Gas adsorption/desorption isotherms were recorded in a Micrometrics ASAP 2020 surface area and pore analyzer. All the gases used were of 99.999% purity.

Synthesis and characterization of H_4BTEB ligand

As shown in Scheme S1, the H_4BTEB was synthesized on a two-step procedure including Sonogashira coupling and hydrolysis reaction:

Tetramethyl 4,4',4'',4'''-(benzene-1,2,4,5-tetrayltetraakis(ethyne-2,1-diyl))tetrabenzoate (**2**). Methyl 4-ethynylbenzoate (**1**) (4.9 g, 30.5 mmol), 1,2,4,5-tetrabromobenzene (2.0 g, 5.1 mmol), $\text{Pd}(\text{PPh}_3)_2\text{Cl}_2$ (0.43 g, 0.6 mmol), PPh_3 (0.32 g, 1.2 mmol), and CuI (0.12 g, 0.6 mmol) were stirred in a deoxygenated mixture of Et_3N (80 mL) and dry THF (80 mL) under N_2 atmosphere. The reaction mixture was heated at $70\text{ }^\circ\text{C}$ for 2 days. After cooling to RT, the mixture was filtered and the solid residue was chromatographed on a silica column (CHCl_3) to give 2.1 g (58 %) of **2** as a golden yellow solid. ^1H NMR (CDCl_3): δ 8.05 (d, 8H), 7.80 (s, 2H), 7.61 (d, 8H), 7.95 (s, 12H) (Fig. S1).

4,4',4'',4'''-(Benzene-1,2,4,5-tetrayltetraakis(ethyne-2,1-diyl))tetrabenzoic acid (H_4BTEB). Compound **2** (2.1 g, 3.0 mmol) was refluxed with 1.4 g of sodium hydroxide in a mixture of THF: MeOH: H_2O (v: v: v = 50 mL : 50 mL : 50 mL) at $70\text{ }^\circ\text{C}$ for 24 h. After cooling to RT, the reaction mixture was concentrated to remove organic solvents by rotary evaporation at reduced pressure. Water (200 mL) was then added to the residue. To this suspension 2 M HCl was slowly added and the pH was adjusted to around 3. The precipitate was filtered and washed with water, and the resulting solid was dried under vacuum at $60\text{ }^\circ\text{C}$ to give H_4BTEB as a yellow solid (1.6g, 83%). ^1H NMR ($\text{DMSO}-d_6$): δ 8.01 (m, 10H), 7.70 (d, 8H) (Fig. S2).

Synthesis of $[\text{Cu}_2(\text{BTEB})(\text{H}_2\text{O})_2]$ (BUT-43)

BUT-43 was synthesized under solvothermal conditions: H_4BTEB (0.11 mmol, 75 mg), $\text{Cu}(\text{OAc})_2\cdot\text{H}_2\text{O}$ (0.25 mmol, 50.0 mg), and acetic acid (1.75 mL) were ultrasonically dissolved in 10 mL of *N,N*-dimethylformamide (DMF) in a 20 mL Pyrex vial and sealed. The reaction system was then heated at $100\text{ }^\circ\text{C}$ for 12 h in an oven. After cooling to RT, the resulting blue crystals of as-synthesized BUT-43 were timely collected by suction filtration, washed with DMF and acetone (38 mg, 41% based on H_4BTEB ligand). PXRD pattern and N_2 adsorption/desorption isotherm of the as-synthesized BUT-43 are shown in Fig. S3 and S4, FT-IR spectrum and TGA curve are shown in Fig. S5 and S7, respectively.

Synthesis of $[\text{Zr}_6\text{O}_4(\text{OH})_8(\text{H}_2\text{O})_4(\text{BTEB})_2]$ (BUT-44)

BUT-44 was also synthesized under solvothermal conditions: H_4BTEB (0.11 mmol, 75 mg), $\text{ZrOCl}_2\cdot 8\text{H}_2\text{O}$ (0.4 mmol, 130 mg), and formic acid (4 mL) were ultrasonically dissolved in 10 mL of NMP in a 20 mL Pyrex vial and sealed. The reaction system was heated at $135\text{ }^\circ\text{C}$ for 24 h in an oven. After cooling to RT, the resulting light yellow crystals of as-synthesized BUT-44 were collected, washed with NMP and acetone, and then dried in air (32 mg, 27% based on

H₄BTEB ligand). PXRD pattern and N₂ adsorption/desorption isotherm of the as-synthesized BUT-44 are shown in Figure 3, FT-IR spectrum and TGA curve are shown in Figures S6 and S8, respectively.

Crystal structure determination

The diffraction data of as-synthesized BUT-43 and -44 were collected in an Agilent Supernova CCD diffractometer equipped with a mirror monochromated enhanced Cu K α radiation ($\lambda = 1.54184 \text{ \AA}$) at 100 K. The datasets were corrected by empirical absorption correction using spherical harmonics, implemented in the SCALE3 ABSPACK scaling algorithm.¹⁴ The structures were solved by direct methods and refined by full-matrix least-squares on F^2 with anisotropic displacement using the SHELXTL software package.¹⁵ Hydrogen atoms of ligands were calculated in ideal positions with isotropic displacement parameters. For BUT-44, hydrogen atoms in coordinated water and hydroxyl groups were not added but were calculated into molecular formula of the crystal data. For these compounds, the volume fractions of disordered solvents in the pores could not be modelled in terms of atomic sites and were treated by using the MASK routine in the Olex2 software package.¹⁶ The topologies of BUT-43 and -44 were calculated with ToposPro¹⁷ and Systre.¹⁸ Crystal parameters and structure refinement are summarized in Table S1 and S2. Crystallographic data of BUT-43 and -44 have been deposited on the Cambridge Crystallographic Data Center (CCDC No. 1842449 and 1842448).

Sample activation and gas adsorption

Before gas adsorption measurements, about 80 mg samples of BUT-43 or BUT-44 crystals were soaked in 15 mL of DMF for 1 day at RT. The samples were collected by decanting and then soaked in 15 mL of acetone for another 3 days, when fresh solvents were exchanged every day. After solvent exchange, the samples were loaded in a sample tube and further activated under high vacuum at an optimized temperature of 150 °C for BUT-43 and 60 °C for BUT-44 for 6 h, respectively. Then, the gas adsorption tests were conducted at 77 K in a liquid nitrogen bath, at 273 K in an ice-water bath, and at 298 K in a water bath.

Stability test

Stability is one of the primary concerns for the practical application of MOFs. To examine the chemical stability of BUT-43 and -44, two as-synthesized samples (100 mg for each) were soaked in water at RT for 72 h as well as in pH = 10 NaOH and 1 M HCl aqueous solutions at RT for 24 h, respectively. Then the treated samples were collected by decanting, washed by water and acetone for PXRD and N₂ adsorption measurements. To assess their thermal stability, the as-synthesized and activated samples of BUT-43 and -44 were characterized by TGA analysis, respectively.

Results and Discussion

Synthesis and crystal structures

As mentioned above, a new MOF composing of ligand BTEB⁴⁻ (Fig. 1a) and paddle-wheel Cu₂(COO)₄ cluster (Fig. 1b) was originally desired, in which a structural interpenetration was expected relying

on the slim feature of the used ligand. By using acetic acid as the competing reagent, block single crystals of BUT-43 suitable for SXRD were obtained from the reaction between H₄BTEB and Cu(OAc)₂·H₂O in DMF. SXRD structure analysis reveals that BUT-43 crystallizes in the monoclinic crystal system of the *C2/c* space group. As expected, the classical Cu₂ cluster exists in the structure of BUT-43, in which two neighboring Cu(II) atoms are bridged by four bimonodentate carboxylate groups from four different BTEB⁴⁻ ligands (the axis sites of the cluster are occupied by two solvent molecules). The lengths of Cu–O bond are in the range of 1.95–1.97 Å, and the Cu...Cu separation is 2.64 Å, all similar to those in reported MOFs based on the Cu₂ cluster.¹⁹ Each Cu₂ cluster connects with four BTEB⁴⁻ ligands, and each ligand links to four Cu₂ clusters to give a single 3D framework. Topologically, the single framework has a *lvt* net with the point symbol of {4².8⁴} when considering both the Cu₂ cluster and the BTEB⁴⁻ ligand as 4-connected nodes (Fig. S9). Due to the large voids in single frameworks and the slight steric hindrance of the slim skeleton of BTEB⁴⁻ ligand, two such identical and independent single frameworks interpenetrate with each other to form the final two-fold interpenetrated framework of BUT-43 (Fig. 1c). As a result of the framework interpenetration, the large 1D rhombic channels (the diagonal distances of the pores are 19.8 and 32.7 Å) in the single framework along the *a*-axes are divided into smaller rhombic channels of two sizes of 13.6 × 19.6 and 7.3 × 8.6 Å², and rhomboid channels (edge distances are 6.4 and 11.6 Å). The total solvent-accessible volume in BUT-43 framework was estimated to be 71.3%, by using PLATON.

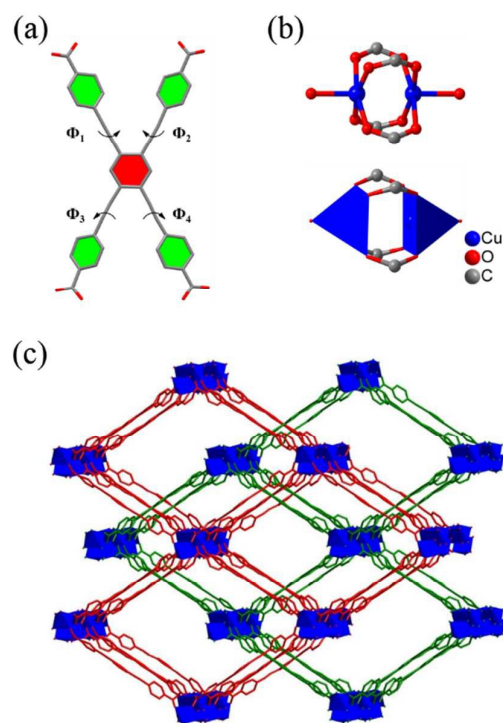


Fig. 1 Structures of ligand BTEB⁴⁻ (a), 4-connected Cu₂ cluster (b), and BUT-43 MOF with a two-fold interpenetrated framework (c). H atoms are omitted for clarity.

Encouraged by the successful trial of BUT-43 with this slim BTEB⁴⁻ ligand based on the typical 4-connected paddle-wheel Cu₂ node, we hope to construct another MOF with Zr₆ cluster of high symmetry and connectivity, which can usually contribute to robust/stable frameworks.^{9b} Simultaneously, an interpenetrated structure is also expected when the versatile Zr₆ cluster encounters this slim ligand. Then, the reaction between H₄BTEB and ZrOCl₂ was performed. At first, we conducted the experiment by using DMF as the solvent in the presence of acetic acid. Only small rod-like crystals were generated. It is regrettable that all attempts to characterize the structure of these tiny crystals through SXRD have failed in our hands so far, due to the too small crystals. Afterwards, we varied the reaction conditions by changing solvents and modulators. Fortunately, bigger needle-like crystals suitable for SXRD were formed in NMP solvent with formic acid as the competing reagent.

SXRD structure analysis shows that BUT-44 crystallizes in the orthorhombic crystal system of *Cmcm* space group. Its framework is based on a hexanuclear Zr₆O₄(OH)₈(H₂O)₄(COO)₈ cluster, which is formed by eight bimonodentate carboxylate groups of different ligands assembling six Zr(IV) atoms (Fig. 2a and 2b); and twelve H₂O/OH⁻ entities complete remaining coordination and account for the charge balance. After careful analysis, the symmetry of this 8-connected Zr₆ core in BUT-44 is found to be different from those in PCN-222,^{12a} NU-1000,^{12b} and BUT-12^{12c}. A slight deformation occurs in the Zr₆ octahedron, with the symmetry reducing from the usual *D_{4h}* to *C₄*. The deformation of this Zr₆ cluster is mainly reflected in that the perpendicular distances from the two crystallographically-independent Zr atoms (Zr1 and Zr2) located on two vertices of the octahedron to the equatorial plane of the cluster (formed by four Zr3 atoms) are not the same. Each BTEB⁴⁻ ligand thus links to four such 8-connected Zr₆ clusters to form an overall 3D structure with 1D rhombic channels along the *a*-axis. From the topological viewpoint, the BTEB⁴⁻ ligand can be seen as a 4-connected linker and the Zr₆ cluster serves as an 8-connected node, the 3D structure of BUT-44 can thus be simplified as a 4,8-connected *scu* net with the point symbol of {4¹⁶.6¹²}{4⁴.6²}₂ (Fig. S11). Similar to that in BUT-43, a two-fold framework interpenetration also occurs in BUT-44, which represents the first example of 4,8-connected Zr(IV)-MOF with an interpenetrated structure. The large 1D rhombic channels (diagonal distances are 16.4 and 36.2 Å) in the single framework are divided into smaller ones of two sizes (13.1 × 18.2 and 10.1 × 10.5 Å²), and rhomboid pores (edge distances are 7.8 and 11.6 Å), respectively (Fig. 2c). The total solvent-accessible volume in the framework of BUT-44 is estimated to be 55.5%, by PLATON.

Carefully analyzing the ligand geometry in BUT-43 and -44, the BTEB⁴⁻ is found to have a "smart" model, where the introduction of ethynyl not only stretches the ligand to a slim one, but also allows the free rotation of four peripheral benzoates (Fig. 1a and 2a). These intrinsic features enable it to well adapt the coordination requirement of metal ions/clusters with different symmetry and connectivity, thereby forming intriguing structures. In BUT-43, the dihedral angles between central benzene ring and four peripheral benzene rings are different ($\Phi_1 = 27.337^\circ$, $\Phi_2 = 38.395^\circ$, $\Phi_3 = 33.541^\circ$, and $\Phi_4 = 14.766^\circ$), while in BUT-44, there only exist two

kinds of rotation angles between the central and four peripheral benzene rings ($\Phi_1 = 46.222^\circ$ and $\Phi_2 = 55.124^\circ$). These two rotation patterns of the ligand BTEB⁴⁻, capable of matching the linkage geometries of Cu₂(COO)₄ and Zr₆O₄(OH)₈(COO)₈ clusters, have thus given rise to BUT-43 and -44, respectively. Furthermore, the less-steric BTEB⁴⁻ ligand and the large hollow pores in single frameworks of both BUT-43 and -44 provide an opportunity for them to generate framework interpenetration, giving rise to the partitioned pores.

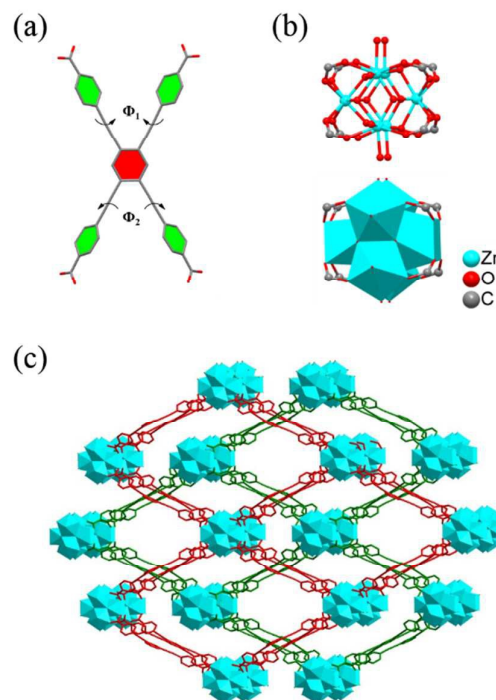


Fig. 2 Structures of ligand BTEB⁴⁻ (a), 8-connected Zr₆ cluster (b), and BUT-44 MOF with a two-fold interpenetrated framework (c). H atoms are omitted for clarity.

Stability and porosity

PXRD analyses were employed to check the phase purity and stability of BUT-43 and -44. The results show that the diffraction patterns of their fresh samples are in good agreement with the simulated ones from single crystal structure data, indicating their pure phases (Fig. 3a and 3b). To examine the chemical stability of BUT-43 and -44, their samples were treated in water for 72 h, pH = 10 NaOH, and 1 M HCl aqueous solutions for 24 h at RT. After immersed in these solutions for given times, the samples were re-collected for further structural characterizations. The measured PXRD patterns of BUT-44 samples after treatments show retained structure, demonstrating its excellent stability (Fig. 3b). By contrast, BUT-43 decomposes in all tests probably due to the weaker Cu–O bonds vulnerable to water molecules, but its framework can remain intact after activation and degassing under above mentioned conditions (Fig. 3a). TGA curves show that the framework of BUT-43 and -44 can be stable up to 300 and 350 °C, respectively (Fig. S7 and S8).

In order to assess their permanent porosity, N₂ adsorption measurements were conducted on BUT-43 and -44 samples pre-activated by solvent exchange and heating under high vacuum (see more details in the Experimental Section). As shown in Fig. 3c, stepwise N₂ adsorption/desorption isotherms are observed for BUT-43, which implies the framework flexibility of this interpenetrated MOF.²⁰ The N₂ uptake is 340 cm³ g⁻¹ (STP) at 1 atm, and the evaluated Brunauer-Emmett-Teller (BET) surface area is 1124 m² g⁻¹. For BUT-44, the N₂ adsorption/desorption at 77 K represents a type I isotherm of microporous materials with the saturated uptake of

326 cm³ g⁻¹ (STP) at 1 atm, and the evaluated BET surface area of 1021 m² g⁻¹ (Fig. 3d). The CO₂ sorption at 195 K on both materials (Fig. S3) has also been performed to examine the rationality of results observed in N₂ adsorption at 77 K, which shows good agreement. Furthermore, N₂ adsorption isotherms of BUT-44 samples treated under different conditions were also measured, and the results show almost the same uptakes as that of the pristine sample (Fig. 3d), which further confirms the framework stability of BUT-44 under neutral, acidic, and weak basic aqueous solutions.

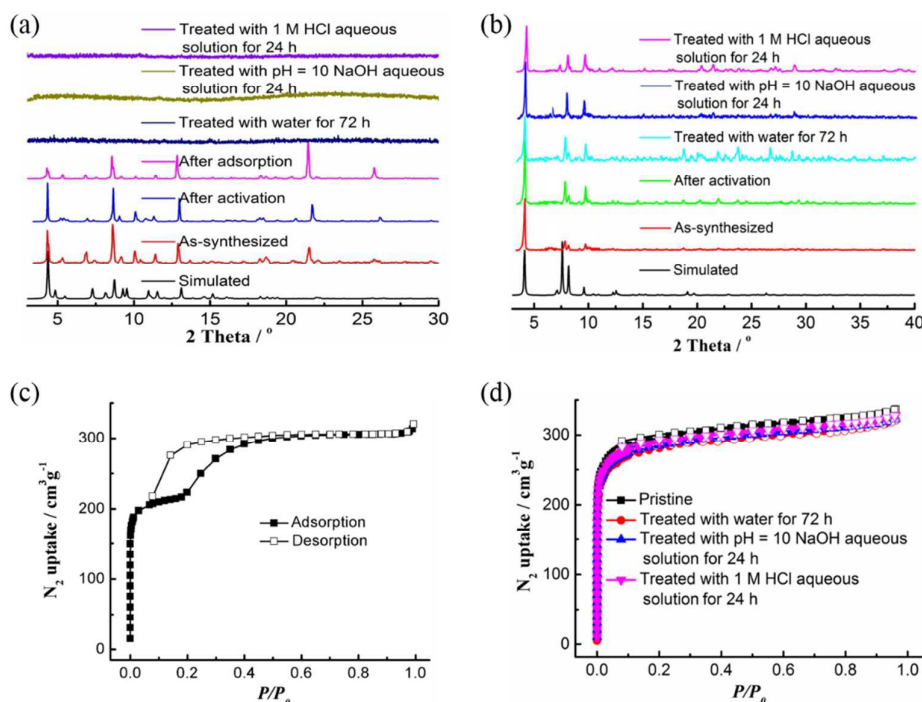


Fig. 3 PXRD patterns of BUT-43 (a) and BUT-44 (b) samples treated under different conditions, and N₂ adsorption/desorption isotherms of pristine BUT-43 (c) and BUT-44 (d) samples treated under different conditions.

Gas selective adsorption

As discussed above, both BUT-43 and -44 have interpenetrated 3D framework. The structural interpenetration leads to their decreased pore size and improved network stability to some extent, making them excellent for gas selective adsorption and separation.

Since the separation of C₂H₂ from CO₂ or CH₄ is very important in industrial productions,²¹ we investigated the performances of BUT-43 and -44 in the adsorptive separation of these gases. The adsorption isotherms of pure C₂H₂, CO₂, and CH₄ in the evacuated BUT-43 and -44 were measured, respectively, and the results are shown in Fig. S12 (at 273 K) and Fig. 4 (at 298 K). As can be seen from these isotherms, the two MOFs have a maximum C₂H₂ uptake of 85.6 and 83.1 cm³ g⁻¹, CO₂ uptake of 51.3 and 52.0 cm³ g⁻¹, and CH₄ uptake of 16.3 and 14.3 cm³ g⁻¹ at 273 K and 1 atm, respectively (Fig. S12a and S12b). At 298 K, there are slight decreases of the adsorbed amounts for C₂H₂ down to 67.7 and 61.9 cm³ g⁻¹, CO₂ to 42.9 and 42.0 cm³ g⁻¹, and CH₄ to 12.7 and 9.5 cm³ g⁻¹, respectively (Fig. 4a and 4b). It was observed that the uptakes of C₂H₂ are significantly higher than those of CO₂ and CH₄, suggesting the

outstanding selective adsorption of C₂H₂ over CO₂ and CH₄. These results indicate the potential applications of BUT-43 and -44 for important C₂H₂/CO₂ and C₂H₂/CH₄ separations. In order to evaluate the feasibility of these MOFs for separations, the adsorption selectivities for the binary C₂H₂/CO₂ and C₂H₂/CH₄ in the two MOFs were evaluated by the ideal adsorbed solution theory (IAST) method²². As shown in Fig. 4c and 4d, the estimated C₂H₂/CO₂ selectivities for an equimolar gas mixture in BUT-43 and -44 at 298 K are in ranges of 3.9–8.4 and 2.7–5.8, respectively. Using the same method, the selectivities of the two MOFs for C₂H₂/CH₄ binary mixture at 298 K were also calculated, to be in ranges of 19.5–35.2 and 18.9–33.5, respectively. At 273 K, the selectivities of BUT-43 for C₂H₂/CO₂ and C₂H₂/CH₄ are 4.3–8.9, 22.2–41.1, and of BUT-44 are 3.7–6.3, 23.5–40.4, higher than those at 298 K (Fig. S12c and S12d).

These data suggest that both BUT-43 and -44 exhibit moderately high selectivities of C₂H₂ over CO₂ and CH₄ at 298 K comparable to some reported MOFs,²³ which could be ascribed to the confined/suitable pores segmented by the network interpenetration and the higher density of acetylenic bonds on the

limited exposed surface of the framework. Compared with BUT-44, the selectivities of BUT-43 (Fig. 4c) are slightly higher, presumably attributing to the different pore size in two MOFs resulting from their different degree of framework interpenetration and rich open metal sites in the latter.

In addition, to evaluate the interaction between gas molecules and the host frameworks, the isosteric heats of adsorption (Q_{st}) for C_2H_2 , CO_2 , and CH_4 in BUT-43 and -44 were calculated by using the Clausius–Clapeyron equation^{22a}, based on their pure component isotherms at 273 and 298 K (Fig. S13). The calculated Q_{st} values for C_2H_2 , CO_2 and CH_4 of BUT-43 are in ranges of 17.1–25.5, 14.9–17.2, and 13.8–14.8, respectively. While those of BUT-44 are 17.1–23.1, 9.0–13.6, and 12.2–13.1, respectively. Among these two MOFs, the

calculated Q_{st} values of BUT-43 are higher, indicating the stronger interaction between its framework and guest molecules.

It should be pointed out that initially we want to explore the specific effect of framework interpenetration on gas selective adsorption of MOFs through designing and constructing BUT-43 and -44. Regrettably, their non-interpenetrated counterparts have not been obtained even after a lot of attempts. Therefore, data of the evidential comparison between their selective gas adsorption capacities is not available now. Further exploration is going on in our lab.

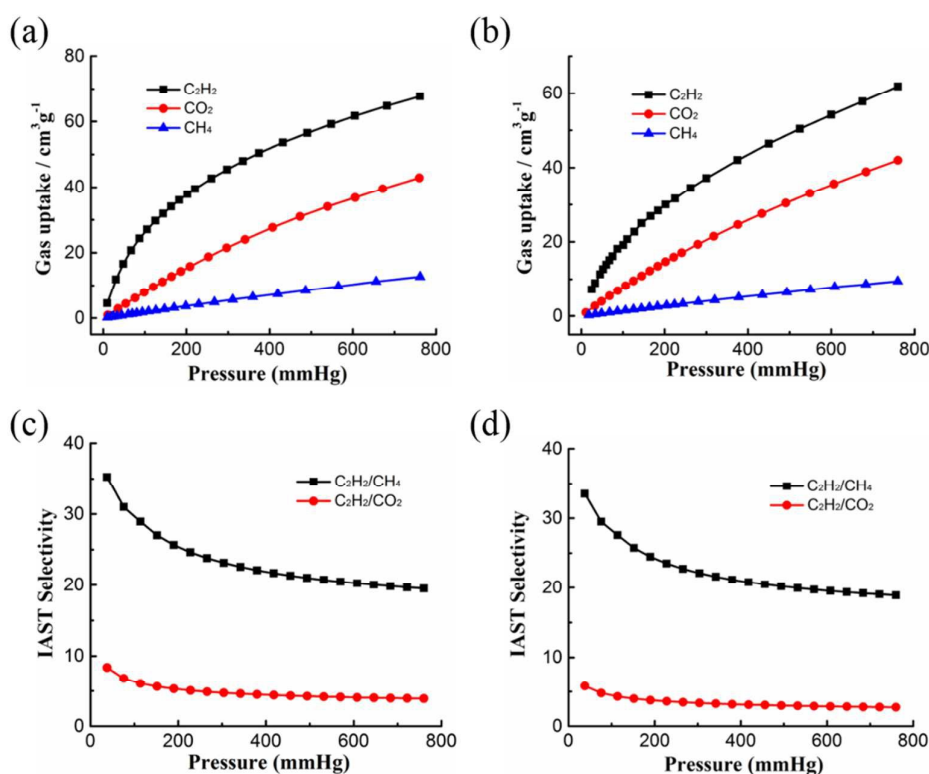


Fig. 4 C_2H_2 , CO_2 , and CH_4 adsorption isotherms recorded at 298 K for BUT-43 (a) and BUT-44 (b); IAST C_2H_2/CH_4 and C_2H_2/CO_2 selectivities in BUT-43 (c) and BUT-44 (d) at 298 K.

Conclusions

In summary, we have successfully constructed two interpenetrated MOFs, by employing a slim ethynyl-based ligand. With typical 4-connected Cu_2 and 8-connected Zr_6 metal-containing clusters, the rational tuning on structures and gas adsorption performance of resulting MOFs was achieved. The $Cu(II)$ -based MOF with higher porosity and large pores could remain intact after removing guest molecules. While the $Zr(IV)$ -based one presents the first example of interpenetrated $Zr(IV)$ -MOF with a 4,8-connected framework structure and can withstand pH = 10 NaOH and 1 M HCl aqueous solutions, being quite stable. Moreover, both MOFs

exhibit moderately high C_2H_2/CO_2 and C_2H_2/CH_4 adsorption selectivities owing to the confined pores resulting from the framework interpenetration and the $C\equiv C$ groups on their pore surfaces, suggesting potential application in gas separation.

Conflicts of interest

There are no conflicts to declare.

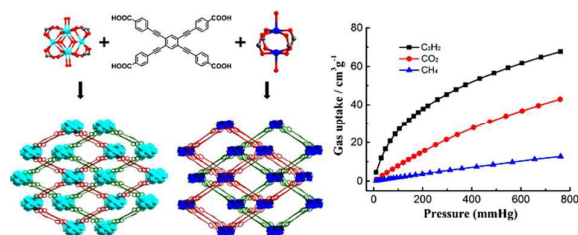
Acknowledgements

We acknowledge financial support from the National Natural Science Foundation (21576006 and 21771012) and the

National Natural Science Fund for Innovative Research Groups (51621003).

Notes and references

- (a) H. Furukawa, K. E. Cordova, M. O'Keeffe, and O. M. Yaghi, *Science*, 2013, **341**, 974–986; (b) Y. Cui, B. Li, H. He, W. Zhou, B. Chen, and G. Qian, *Acc. Chem. Res.*, 2016, **49**, 483–493; (c) A. J. Howarth, Y. Liu, P. Li, Z. Li, T. C. Wang, J. T. Hupp, and O. K. Farha, *Nat. Rev. Mater.*, 2016, **1**, 15018.
- (a) J.-R. Li, J. Sculley, and H.-C. Zhou, *Chem. Rev.*, 2012, **112**, 869–932; (b) Z. Hu, B. J. Deibert, and J. Li, *Chem. Soc. Rev.*, 2014, **43**, 5815–5840; (c) J. Yu, L.-H. Xie, J.-R. Li, Y. Ma, J. M. Seminario, and P. B. Balbuena, *Chem. Rev.*, 2017, **117**, 9674–9754; (d) L. Zeng, X. Guo, C. He, and C. Duan, *ACS Catal.*, 2016, **6**, 7935–7947; (e) K.-J. Chen, H. S. Scott, David G. Madden, T. Pham, A. Kumar, A. Bajpai, M. Lusi, K. A. Forrest, B. Space, J. J. Perry IV, and M. J. Zaworotko, *Chem*, 2016, **1**, 753–765; (f) P. Li, Y. He, Y. Zhao, L. Weng, H. Wang, R. Krishna, H. Wu, W. Zhou, M. O'Keeffe, Y. Han, and B. Chen, *Angew. Chem.*, 2015, **127**, 584–587; (g) H. Xu, Y. He, Z. Zhang, S. Xiang, J. Cai, Y. Cui, Y. Yang, G. Qian and B. Chen, *J. Mater. Chem. A*, 2013, **1**, 77–81.
- (a) T. R. Cook, Y. R. Zheng and P. J. Stang, *Chem. Rev.*, 2013, **113**, 734–777; (b) T. Zhao, C. Heering, I. Boldog, K. V. Domasevitch, and C. Janiak, *CrystEngComm*, 2017, **19**, 776–780.
- S. B. Kalidindi, S. Nayak, M. E. Briggs, S. Jansat, A. P. Katsoulidis, G. J. Miller, J. E. Warren, D. Antypov, F. Corà, B. Slater, M. R. Prestly, C. Martí-Gastaldo, and M. J. Rosseinsky, *Angew. Chem., Int. Ed.*, 2015, **54**, 221–226;
- (a) O. K. Farha, C. D. Malliakas, M. G. Kanatzidis, and J. T. Hupp, *J. Am. Chem. Soc.*, 2010, **132**, 950–952; (b) Z. Zhang, S. Xiang, K. Hong, C. D. Madhab, H. D. Arman, M. Garcia, J. U. Mondal, K. M. Thomas, and B. Chen, *Inorg. Chem.*, 2012, **51**, 4947–4953; (c) H.-L. Jiang, T. A. Makal, and H.-C. Zhou, *Coord. Chem. Rev.*, 2013, **257**, 2232–2249.
- (a) S. Couck, J. Denayer, G. Baron, T. Rémy, J. Gascon, and F. Kapteijn, *J. Am. Chem. Soc.*, 2009, **131**, 6326–6327; (b) V. Safarifard, S. Rodriguez-Hermida, V. Guillermin, I. Imaz, M. Bigdeli, A. A. Tehrani, J. Juanhuix, A. Morsali, M. E. Casco, J. Silvestre-Albero, E. V. Ramos-Fernandez, and D. Maspocho, *Cryst. Growth Des.*, 2016, **16**, 6016–6023; (c) A. Torrisi, R. Bell, and C. Mellot-Draznieks, *Cryst. Growth Des.*, 2010, **10**, 2839–2841; (d) Y. Hu, S. Xiang, W. Zhang, Z. Zhang, L. Wang, J. Bai, and B. Chen, *Chem. Commun.*, 2009, **48**, 7551–7553; (e) B. Zheng, R. Yun, J. Bai, Z. Lu, L. Du, and Y. Li, *Inorg. Chem.*, 2013, **52**, 2823–2829.
- (a) M. Jiang, B. Li, X. Cui, Q. Yang, Z. Bao, Y. Yang, H. Wu, W. Zhou, B. Chen, and H. Xing, *ACS Appl. Mater. Interfaces*, 2018, **10**, 16628–16635; (b) P. Nugent, Y. Belmabkhout, S. D. Burd, A. J. Cairns, R. Luebke, K. Forrest, T. Pham, S. Ma, B. Space, L. Wojtas, M. Eddaoudi, and M. J. Zaworotko, *Nature*, 2013, **495**, 80–84; (c) H. S. Scott, N. Ogiwara, K.-J. Chen, D. G. Madden, T. Pham, K. Forrest, B. Space, S. Horike, J. J. Perry IV, S. Kitagawa and M. J. Zaworotko, *Chem. Sci.*, 2016, **7**, 5470–5476.
- (a) M. O'Keeffe, and O. M. Yaghi, *Chem. Rev.*, 2012, **112**, 675–702; (b) S. T. Zheng, T. Wu, C. Chou, A. Fuhr, P. Y. Feng, and X. H. Bu, *J. Am. Chem. Soc.*, 2012, **134**, 4517–4520; (c) L.-D. Lin, X.-X. Li, Y.-J. Qi, X. Ma, and S.-T. Zheng, *Inorg. Chem.*, 2017, **56**, 4635–4642; (d) X.-Y. Li, Y.-Z. Li, Y. Yang, L. Hou, Y.-Y. Wang and Z. Zhu, *Chem. Commun.*, 2017, **53**, 12970–12973; (e) H.-H. Wang, L.-N. Jia, L. Hou, W.-J. Shi, Z. Zhu, and Y.-Y. Wang, *Inorg. Chem.*, 2015, **54**, 1841–1846.
- (a) K.-J. Chen, D. G. Madden, T. Pham, K. A. Forrest, A. Kumar, Q.-Y. Yang, W. Xue, B. Space, J. J. Perry, J.-P. Zhang, X.-M. Chen, and M. J. Zaworotko, *Angew. Chem., Int. Ed.*, 2016, **55**, 10268–10272; (b) Y. Bai, Y. Dou, L. H. Xie, W. Rutledge, J.-R. Li, and H.-C. Zhou, *Chem. Soc. Rev.*, 2016, **45**, 2327–2367.
- (a) J. H. Cavka, S. Jakobsen, U. Olsbye, N. Guillou, C. Lamberti, S. Bordiga, and K. P. Lillerud, *J. Am. Chem. Soc.*, 2008, **130**, 13850–13851; (b) T.-H. Chen, I. Popov, and O. Š. Miljanić, *Chem.-Eur. J.*, 2017, **23**, 286–290; (c) H. Furukawa, F. Gándara, Y.-B. Zhang, J. Jiang, W. L. Queen, M. R. Hudson, and O. M. Yaghi, *J. Am. Chem. Soc.*, 2014, **136**, 4369–4381; (d) R. Wang, Z. Wang, Y. Xu, F. Dai, L. Zhang, and D. Sun, *Inorg. Chem.*, 2014, **53**, 7086–7088; (e) D. Feng, K. Wang, J. Su, T.-F. Liu, J. Park, Z. Wei, M. Bosch, A. Yakovenko, X. Zou, and H.-C. Zhou, *Angew. Chem., Int. Ed.*, 2015, **54**, 149–154; (f) T. He, Y.-Z. Zhang, X.-J. Kong, J. Yu, X.-L. Lv, Y. Wu, Z.-J. Guo, and J.-R. Li, *ACS Appl. Mater. Interfaces*, 2018, **10**, 16650–16659.
- (a) J. Lee, O. K. Farha, J. Roberts, K. A. Scheidt, S. T. Nguyen, and J. T. Hupp, *Chem. Soc. Rev.*, 2009, **38**, 1450–1459; (b) B. Chen, M. Eddaoudi, S. T. Hyde, M. O'Keeffe, and O. M. Yaghi, *Science*, 2001, **291**, 1021–1023.
- (a) D. Feng, Z.-Y. Gu, J.-R. Li, H.-L. Jiang, Z. Wei, and H.-C. Zhou, *Angew. Chem., Int. Ed.*, 2012, **51**, 10307–10310; (b) J. E. Mondloch, W. Bury, D. Fairen-Jimenez, S. Kwon, E. J. DeMarco, M. H. Weston, A. A. Sarjeant, S. T. Nguyen, P. C. Stair, R. Q. Snurr, O. K. Farha, and J. T. Hupp, *J. Am. Chem. Soc.*, 2013, **135**, 10294–10297; (c) B. Wang, X.-L. Lv, D. Feng, L.-H. Xie, J. Zhang, M. Li, Y. Xie, J.-R. Li, and H.-C. Zhou, *J. Am. Chem. Soc.*, 2016, **138**, 6204–6216.
- (a) M. J. Rosseinsky, C. G. Perkins, J. E. Warren, K. E. Jelfs, and P. Boldrin, *U.S. Pat. Appl. Publ.*, 2015, US 20150231600; (b) M. J. Rosseinsky, C. G. Perkins, J. E. Warren, K. E. Jelfs, and P. Boldrin, *PCT Int. Appl.*, 2014, WO 2014033481.
- G. M. Sheldrick, SHELXTL 2008/4, *Structure determination software suite*; Bruker AXS Inc.: Madison, WI.
- SCALE3 ABSPACK scaling algorithm. CrysAlis RED, Oxford Diffraction Ltd., Version 1.171.32.38.
- O. V. Dolomanov, L. J. Bourhis, R. J. Gildea, J. A. K. Howard, and H. Puschmann, *J. Appl. Cryst.* 2009, **42**, 339–341.
- V. A. Blatov, A. P. Shevchenko, D. M. Proserpio, *Cryst. Growth Des.* 2014, **14**, 3576–3586.
- O. Delgado-Friedrichs, M. O'Keeffe, *Acta Crystallogr. Sect. A* 2003, **59**, 351–360.
- Y. Chen, B. Wang, X. Wang, L.-H. Xie, J. Li, Y. Xie, and J.-R. Li, *ACS Appl. Mater. Interfaces*, 2017, **9**, 27027–27035.
- P. Schmieider, M. Grzywa, D. Denysenko, M. Hambach, and D. Volkmer, *Dalton Trans.*, 2015, **44**, 13060–13070.
- (a) R. Matsuda, R. Kitaura, S. Kitagawa, Y. Kubota, R. V. Belosludov, T. C. Kobayashi, H. Sakamoto, T. Chiba, M. Takata, Y. Kawazoe, and Y. Mita, *Nature*, 2005, **436**, 238–241; (b) P. Li, Y. He, Y. Zhao, L. Weng, H. Wang, R. Krishna, H. Wu, W. Zhou, M. O'Keeffe, Y. Han, and B. Chen, *Angew. Chem., Int. Ed.*, 2014, **53**, 1–5.
- (a) L.-H. Xie, and M. P. Suh, *Chem. Eur. J.* 2013, **19**, 11590–11597; (b) J. Duan, M. Higuchi, J. Zheng, S. Noro, I. Chang, K. Hyeon-Deuk, S. Mathew, S. Kusaka, E. Sivaniah, R. Matsuda, S. Sakaki, and S. Kitagawa, *J. Am. Chem. Soc.*, 2017, **139**, 11567–11583; (c) M. L. Foo, R. Matsuda, Y. Hijikata, R. Krishna, H. Sato, S. Horike, A. Hori, J. Duan, Y. Sato, Y. Kubota, M. Takata, and S. Kitagawa, *J. Am. Chem. Soc.*, 2016, **138**, 3022–3030; (d) B. Li, Y. Zhang, R. Krishna, K. Yao, Y. Han, Z. Wu, D. Ma, Z. Shi, T. Pham, B. Space, J. Liu, P. K. Thallapally, J. Liu, M. Chrzanowski, and S. Ma, *J. Am. Chem. Soc.*, 2014, **136**, 8654–8660; (e) J. Duan, W. Jin, and R. Krishna, *Inorg. Chem.*, 2015, **54**, 4279–4284.
- (a) J.-X. Ma, J. Guo, H. Wang, B. Li, T. Yang, and B. Chen, *Inorg. Chem.*, 2017, **56**, 7145–7150; (b) L. Zhang, C. Zou, M. Zhao, K. Jiang, R. Lin, Y. He, C.-D. Wu, Y. Cui, B. Chen, and G. Qian, *Cryst. Growth Des.*, 2016, **16**, 7194–7197.



Structural tuning and selective gas adsorption of two interpenetrated metal-organic frameworks with a slim ethynyl-based ligand was identified.